PSFC/JA-11-37

Feasibility Study for a Correlation Electron Cyclotron Emission Turbulence Diagnostic Based on Nonlinear Gyrokinetic Simulations

White, A.E., Howard, N.T., Mikkelsen, D.R.*, Greenwald, M., Candy, J.**, Waltz, R.E. **

* Princeton Plasma Physics Laboratory
** General Atomics

January, 2012

Plasma Science and Fusion Center
Massachusetts Institute of Technology
Cambridge MA 02139 USA

This work was supported by the U.S. Department of Energy, Grant No. DE-FC02-99ER54512-CMOD.

Feasibility Study for a Correlation Electron Cyclotron Emission Turbulence Diagnostic Based on Nonlinear Gyrokinetic Simulations

A. E. White[1], N. T. Howard[1], D. R. Mikkelsen[2], M. Greenwald[1], J. Candy[3], R. E. Waltz[3]

[1] Massachusetts Institute of Technology, USA
[2] Princeton Plasma Physics Laboratory, USA
[3] General Atomics, P.O. Box 85608, San Diego, CA 92186-5608

E-mail: whitea@mit.edu

Abstract. This paper describes the use of nonlinear gyrokinetic simulations to assess the feasibility of a new correlation electron cyclotron emission (CECE) diagnostic that has been proposed for the Alcator C-Mod tokamak [E. Marmar *et al* 2009 Nucl. Fusion 49, 104014]. The present work is based on a series of simulations performed with the GYRO code [J. Candy and R. E. Waltz, 2003 Journal of Computational Physics 186, 545]. The simulations are used to predict ranges of fluctuation level, peak poloidal wavenumber and radial correlation length of electron temperature fluctuations in the core of the plasma. The impact of antenna pattern and poloidal viewing location on measurable turbulence characteristics is addressed using synthetic diagnostics. An upper limit on the CECE sample volume size is determined. The modeling results show that a CECE diagnostic capable of measuring transport-relevant, long-wavelength ($k_\theta \rho_s < 0.5$) electron temperature fluctuations is feasible at Alcator C-Mod.

1. Introduction

The observed levels of transport in tokamak plasmas typically exceed neoclassical theory predictions by an order of magnitude or more, and turbulence is believed to play a large role in determining this transport [1]. Advanced fluctuation diagnostics used to study core turbulence in tokamaks are important to the development of magnetic confinement fusion. The best available physical model for turbulence and turbulent-transport in tokamaks is gyrokinetic theory [2]. Nonlinear gyrokinetic simulations solve the coupled gyrokinetic-Maxwell's equations and can match the experimental levels of transport observed in tokamaks [3, 4]. By using these gyrokinetic simulations as tools, new experiments and new diagnostics can be designed explicitly to test gyrokinetics [5].

Tokamak diagnostic design and feasibility studies employing advanced simulations as tools are common (e.g. assessment of Motional Stark Effect [6] and Charge Exchange Recombination Spectroscopy [7] for ITER). Yet for turbulence diagnostics, detailed modeling using nonlinear gyrokinetic simulations has not been previously performed as part of a diagnostic design and feasibility study. This is for two reasons. First, a great deal of fluctuation diagnostic design can be done qualitatively using simple estimates of the fluctuation level and the underlying turbulent wavenumber spectrum. These methods are often sufficient. Second, running nonlinear gyrokinetic simulations is a nontrivial and time-consuming endeavor. In addition, only very recently have nonlinear gyrokinetic simulations matured to a point where realistic predictions for turbulence characteristics are possible [4].

Moving beyond an empirical feasibility study to a gyrokinetic code-based feasibility study is motivated at Alcator C-Mod by past attempts to measure electron temperature fluctuations. The multi-channel radiometer used in the past experimental study at Alcator C-Mod had been designed with turbulence measurements in mind [8, 9], but no turbulent fluctuations above the noise level were observed [10]. The turbulence characteristics that were used to inform that diagnostic design were not motivated by gyrokinetic theory, but instead were taken from past experiments. In this paper, we use gyrokinetic codes to help understand the old result and to explore the feasibility of a new turbulence diagnostic proposed for Alcator C-Mod. The methods described in this paper may be applied to turbulence diagnostic design at other existing and future tokamaks, such as ITER.

In the present work, nonlinear gyrokinetic simulations [4] and synthetic diagnostic models [11, 12] are used to quantitatively predict electron temperature fluctuations in the core plasma at Alcator C-Mod [13]. The simulations are performed with the nonlinear gyrokinetic code GYRO [14]. GYRO simulations can predict transport due to turbulence that is in good agreement with experimental levels to within experimental uncertainties [3, 12, 15, 16, 17]. We note that there are still outstanding points of disagreement between simulations and experiment [4, 12, 17, 18] and that the validation of gyrokinetic codes remains an active area of research.

The purpose of this work is not to test or validate a gyrokinetic code. This work

is performed to determine whether or not a proposed correlation electron cyclotron emission (CECE) diagnostic is feasible at Alcator C-Mod. GYRO is used to predict the turbulence fluctuation level, radial correlation length and wavenumber spectrum of the fluctuations. These predicted turbulence characteristics are then used to constrain the design of the diagnostic. The predicted turbulence characteristics will determine the maximum allowable sample volume size, the acceptable upper limits on the sensitivity of the diagnostic, as well the details of the receiver electronics. In order for the proposed CECE diagnostic to be feasible, turbulence predicted by gyrokinetic simulations must be measurable, given constraints imposed by principles of radiometer-based ECE measurements.

This paper is organized as follows: Section 2 describes radiometer-based CECE diagnostics and discusses how predicted turbulence characteristics will constrain their design. Section 3 describes the general simulation approach. Section 4 describes local nonlinear GYRO simulations and synthetic diagnostic modeling. Section 5 describes global simulation results and the sensitivity of predicted turbulence characteristics. Section 6 summarizes the modeling results and discusses future work.

2. Requirements for a CECE Turbulence Diagnostic

2.1. Sensitivity of ECE diagnostics to low-level temperature fluctuations

Detection of optically thick 2nd harmonic EC emission is a standard technique for measurement of electron temperature in tokamaks [19]. The 2nd harmonic EC emission at Alcator C-Mod is optically thick and accessible from the outboard mid-plane in standard operating conditions, and there are three ECE diagnostics in place that are routinely used: a Michelson interferometer [20], a Grating Polychromator (GPC) system [21] and a 32 channel radiometer [8, 9]. The use of ECE radiometers as profile and fluctuation diagnostics has been reviewed in the past [22, 23].

A single ECE radiometer channel has excellent spatial and temporal resolution, but there is an inherent limitation on the lowest level amplitude change in electron temperature that can be detected. The sensitivity limit for a single radiometer channel is given as

$$(\delta T/T)^2 = 2B_{vid}/B_{if} \tag{1}$$

where B_{vid} is the video bandwidth and B_{if} is the intermediate frequency (IF) bandwidth of the radiometer [24, 23]. This sensitivity limit given by Eqn. 1 is typically called the thermal noise level. Since the radial resolution of an ECE radiometer is determined by a combination of the ECE linewidth and the IF bandwidth, for profile ECE radiometers it is best to use an IF bandwidth comparable to the ECE linewidth. To minimize the thermal noise level, a narrow video bandwidth is chosen. In order to use a Correlation ECE (CECE) radiometer as a turbulence diagnostic, there are other constraints on the choice of IF and video bandwidths that must be considered.

The proposed CECE diagnostic for turbulence measurements at Alcator C-Mod will implement the spectral decorrelation technique first pioneered at the TEXT tokamak [25, 23]. With this method, two ECE radiometer signals with intermediate frequency filters that are disjoint in frequency space are correlated. If the filters are separated by less than the correlation length of the turbulence, information about the underlying electron temperature fluctuations can be recovered. When the bandwidth of the fluctuations of interest, B_{sig} is comparable to B_{vid}, the turbulence can only be measured by averaging over time Δt and calculating the cross-correlation coefficient. The sensitivity is then given by

$$(\delta T/T)^2 = \sqrt{1/N}\,(2B_{sig}/B_{if}) \tag{2}$$

where the number of independent samples used to calculate the cross-correlation is $N = 2B_{vid}\Delta t$ [25, 26]. In cases where the bandwidth of the turbulence, B_{sig}, is small compared to B_{vid}, it is possible to recover a limited time history of the fluctuations [17]. This is because the sensitivity to low amplitude fluctuations improves when $B_{sig} < B_{vid}$ [27].

2.2. Constraints on diagnostic design imposed by turbulence characteristics

To determine whether or not a turbulence diagnostic is feasible, it is necessary to know expected ranges for at least three turbulence parameters: fluctuation level, $\tilde{T}_e/T_e$, peak poloidal wavenumber, $k_\theta \rho_s$, and the radial correlation length, L_r. We discuss below how predicted turbulence parameters translate into CECE diagnostic design considerations.

2.2.1. Wavenumber spectrum For turbulence measurements, it is essential that the spatial resolution of the diagnostic be fine enough to resolve the small spatial scales associated with the fluctuations. For the proposed CECE diagnostic, the spatial resolution in the poloidal and toroidal directions is determined by the antenna pattern of the Gaussian beam used to couple the emission from the plasma to the radiometer receiver [23]. The sample volume is roughly in the shape of a pill-box with a larger vertical extent compared to the radial extent. The spatial resolution in the radial direction is determined a combination of the intermediate frequency filter bandwidth and the line-width of the EC emission [23]. The vertical extent of the sample volume, called the spot-size, d, determines the poloidal wavenumber sensitivity of the CECE diagnostic. If the spot-size is too large, a CECE diagnostic will not be able to resolve the turbulence because the diagnostic will only be sensitive to fluctuations with wavenumbers

$$k_\theta < 2\pi/d \tag{3}$$

.

The deleterious effects of finite sample volume size on the measurements can be modeled quantitatively with synthetic diagnostics using a point spread function (PSF) once the wavenumber spectrum of the turbulence is known [28, 12]. The wavenumber spectrum of the fluctuation power, $\tilde{T}_e/T_e$ as a function of the normalized wavenumber

$k_\theta \rho_s$, and the peak value, $k_\theta \rho_s^{peak}$, can be obtained from GYRO simulations [12]. Here, $k_\theta \rho_s < 1.0$ indicates that the turbulence is long wavelength, with scale size larger than an ion sound gyroradius, $\rho_s = c_s/\Omega_{ci}$, with sound speed $c_s = \sqrt{T_e/m_i}$ and $\Omega_{ci} = eB/m_i c$.

The spot-size can be quantified as twice the beam waist, $d = 2w_0$, where the beam waist is defined as the radius (w_0) at which the electric field falls to $1/e$ relative to the on-axis value [29]. A practical limit on the minimum achievable spot-size beam waist of the Gaussian antenna pattern is set by the wavelength of the emission of interest. On Alcator C-Mod the standard operating magnetic field of 5.4 T on axis gives a frequency range of $240 < 2f_{ce} < 290$ GHz for 2nd harmonic ECE in the core region of interest, $0.4 < \rho < 0.8$. The vacuum wavelength is therefore in the range $1.0 < \lambda_0 < 1.2$ millimeters. As long as $w_0/\lambda > 1.6$, variations in the beam radius along the axis (i.e. the beam divergence) will not occur over distances comparable to the vacuum wavelength of the beam [29] and standard Gaussian optical arrangements can be used [23]. This sets a practical lower limit of $d = 2w_0 < 3.84$ millimeters for the spot-size of the diagnostic at Alcator C-Mod. If GYRO simulations predict that the wavenumber spectrum of electron temperature fluctuations peaks at wavenumbers so high that a spot-size smaller than the practical minimum spot-size is needed, then the measurement is not feasible. In addition to the spot-size requirements, the correlation analysis used with a CECE diagnostic to measure turbulence must also be considered, as we now discuss.

2.2.2. Radial correlation length A radiometer-based CECE measurement of $\tilde{T}_e/T_e$ requires two radially separated sample volumes in order to measure the fluctuation amplitude and frequency power spectrum via cross-correlation analysis [25]. Because of the two sample volumes are separated radially, the spatial decorrelation of the turbulence is also important. The spatial decorrelation of the turbulence is quantified by the radial correlation length, L_r, which is expected to scale as $5 - 10\rho_s$ based on past experiments [30]. Note from Eqn. 2 that the sensitivity of the CECE diagnostic can be improved somewhat by changing the ratio of B_{if} and B_{vid} in the radiometer receiver, but for turbulence measurements, there is limited flexibility in these choices. This is because two neighboring intermediate frequency filters need to be disjoint in frequency space to decorrelate the thermal noise, but they must also be separated by less than the correlation length of the turbulence. This means the IF bandwidth, B_{if}, cannot be made so large that this constraint is violated. If the predicted correlation length of the turbulence is so small that in order to resolve the fluctuations with a CECE receiver one is forced to choose an IF bandwidth that increases the sensitivity limit (Eqn. 2) above the predicted fluctuation level, then the measurement is not feasible.

For a CECE radiometer to be used at a turbulence diagnostic, it is desirable to use a narrow intermediate frequency filter bandwidth, B_{if}, so that two channels can be separated by less than a turbulence correlation length. It is also desirable to use a wide video bandwidth,B_{vid}, to resolve broad turbulence spectra, which can extend up to a MHz in the laboratory frame due to Doppler shifts. Because of this, the thermal noise

level cannot be significantly reduced by adjustment of B_{vid}/B_{if} without compromising spatial and spectral resolution. The sensitivity to low amplitude, broadband fluctuations can only be significantly improved by cross correlating two radiometer channels that have uncorrelated thermal noise [31, 25].

2.2.3. Fluctuation Level For a CECE diagnostic, it is critical that the diagnostic be sensitive to broadband, low-amplitude fluctuations of electron temperature fluctuations $\tilde{T}_e$. As an example of the sensitivity possible, consider the following parameters: a 400 ms time average and values of $B_{sig} = 400$ kHz, $B_{if} = 90$ MHz, and $B_{vid} = 1$ MHz. The sensitivity of a CECE measurement for these parameters is $\approx 0.3\%$, according to Eqn. 2. The normalized fluctuation level, $\tilde{T}_e/T_e$, for core plasmas is expected to be on the order of $0.1 - 1.0\%$ based on past experiments [23, 17], but note the fluctuation level has not yet been measured in Alcator C-Mod. In this study, the fluctuation level is predicted for Alcator C-Mod using the GYRO code. If the predicted fluctuation level is below a practical minimum achievable sensitivity limit of $0.3\% - 0.4\%$, then the measurement is not feasible.

3. General Simulation Approach

For this diagnostic feasibility study we define a realistic simulation as one that uses experimentally accessible ranges of plasma parameters as input and predicts transport levels that are consistent with experimentally inferred transport levels. This second requirement is important because an overestimate of transport levels will translate into an overestimate of the measurable turbulence amplitude, which would provide too optimistic a prediction for the capabilities of a new turbulence diagnostic. It is also necessary to ensure that the predicted wavenumber spectrum of the turbulence does not peak at an unrealistically low (high) wavenumber, which will also lead to too optimistic (pessimistic) a feasibility assessment, via Eqn. 3. This is difficult to track, because predicting how much transport is driven by long and short wavelengths, and the interplay between different regions of k-space, is an active area of research requiring extremely expensive simulations that we do not employ here [32, 33].

For this study, a database of nonlinear GYRO simulations of Alcator C-Mod plasmas was compiled. A large set of nonlinear global GYRO simulations was available from a separate study of impurity transport [34], and a series of local simulations for the synthetic diagnostic modeling were run specifically for the CECE feasibility study. The plasmas simulated represent typical Alcator C-Mod L-mode plasmas, heated with 1-2 MW of Ion Cyclotron Resonance Heating (ICRH). Figure 1 shows smoothed curve-fits (combination of spline for the core and polynomial for the edge) to the experimentally measured electron density and temperature profiles from four example discharges that are part of a plasma current scan, with $I_p = 0.6, 0.8, 1.0$ and 1.2 MA. In the figure, (a) electron density, n_e, and (b) electron temperature, T_e, are shown over the region $0.0 < \rho < 1.0$. The radial profiles normalized gradient scale lengths, (c)

$a/L_n = -(a/n)(dn/dr)$ and (d) $a/L_{Te} = -(a/T_e)(dT_e/dr)$, (e) safety factor, q, and (f) magnetic shear, $\hat{s}$, are shown over a smaller radial region relevant for the turbulence simulations, $0.2 < \rho < 0.6$.

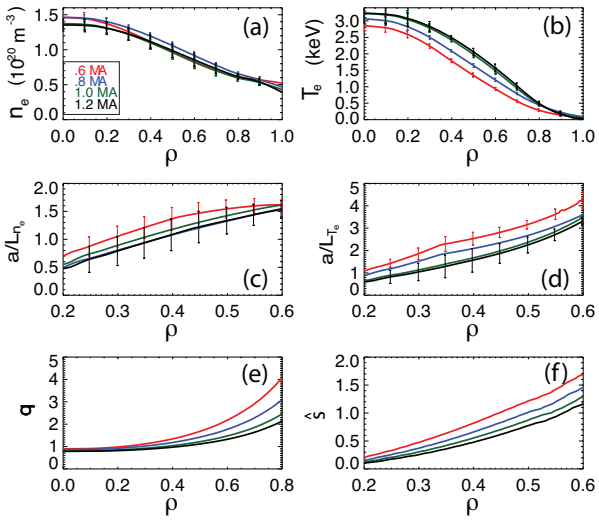

Figure 1. (Colour online) Experimental profiles from typical Alcator C-Mod L-mode plasmas. (a) The electron density, n_e, and (b) electron temperature, T_e, are shown over the region $0.0 < \rho < 1.0$. The radial profiles normalized gradient scale lengths, (c) $a/L_n = -(a/n)(dn/dr)$ and (d) $a/L_{Te} = -(a/T_e)(dT_e/dr)$, (e) safety factor, q, and (f) magnetic shear, $\hat{s}$, are shown over a smaller radial region relevant for the turbulence simulations, $0.2 < \rho < 0.6$

The electron density and electron temperature radial profiles are measured with a Thomson Scattering (TS) system [35]. Typical error bars on these measurements are 15%. Electron temperature profiles are also measured with a 32 channel ECE radiometer [8, 9] and a Grating Polychromator (GPC) ECE system [21]. Typical error bars on these measurements are 10%. Ion temperature profile and velocity profiles, from which E_r and the $E \times B$ shearing rate can be calculated, are usually available from a high resolution x-ray spectrometer [36]. However, these data were not available for this study. The experimental q-profile and shear profile, $\hat{s} = r(d \ln q/dr)$, are calculated from a EFIT [37] equilibrium reconstruction constrained using external magnetic measurements. Uncertainty in q and $\hat{s}$ is roughly 20%. In Table 1 the L-mode experimental parameter ranges covered in the simulation database are summarized.

The preparation of an input file for GYRO using experimental parameters is performed using standard methods implemented previously at Alcator C-Mod [16]: the output of TRANSP [38, 39] is used with the data translator (trgk) developed at PPPL to produce the input files used by GYRO for both local and global simulations.

In this study, TRANSP is used to calculate the ion temperature profile, constrained by neutron measurements [16]. The value of $E \times B$ shear (when used in the local simulations) is taken from a similar L-mode plasma where E_r information was available.

TRANSP is also used to calculate the experimental transport levels that are used to determine whether or not GYRO calculated transport levels are realistic. Output

Table 1. Experimental parameters for the typical L-mode Alcator C-Mod plasmas heated with 1-2 MW of ICRH that are considered in this feasibility study.

	L-mode
B_t	5.4 T
I_p	0.6-1.2 MA
P_{ICRF}	1-2 MW
$\langle n_e \rangle$	$0.7 - 1.0 \times 10^{20}$ m^{-3}
$n_e(0)$	$1.0 - 1.5 \times 10^{20}$ m^{-3}
$T_e(0)$	$3.0 - 3.2$ keV
$T_i(0)$	$1.6 - 3.0$ keV
q_{95}	3.2-5.8
κ	1.6
δ	0.4

from TRANSP from long steady periods of the discharge are time-averaged in order to estimate uncertainties in calculated heat fluxes. These uncertainties in the TRANSP outputs are due to variations in the experimental profiles in time, and provide a reasonable estimate of the experimental uncertainties in the reported heat flux. For the plasmas here, we find uncertainties for TRANSP ion and electron heat fluxes in the range $10 - 15\%$. Other methods of estimated the uncertainties in TRANSP outputs have been discussed elsewhere [40].

4. Results from Local GYRO Simulations

In order to determine whether or not a CECE diagnostic is feasible, the nonlinear GYRO simulations are used to obtain predicted ranges for three turbulence parameters: fluctuation level, $\tilde{T}_e/T_e$, peak poloidal wavenumber, $k_\theta \rho_s$, and the radial correlation length, L_r. More than thirty GYRO simulations were used in this study, including local and global simulations. Local simulation results are used with synthetic diagnostic models in order to generate quantitive predictions for the required CECE spot-size and the effect of an off mid-plane view. One local simulation is discussed here in detail. Global simulations are discussed later in Section 6.

The local simulation of interest was prepared using data from C-Mod discharge 1100308003 ($B_T = 5.46$ T, $I_p = 0.8$ MA) at $t = 1.0$ sec during the current flattop. This is a typical sawtoothing L-mode plasma ($q_0 = 1$, $q_{95} = 4.5$) with $P_{RF} = 1.2$ MW of Ion Cyclotron Resonance Heating. The central density is $n_e(0) = 1.4 \times 10^{20}$ m^{-3}, line averaged density $\langle n_e \rangle = 0.95 \times 10^{20}$ m^{-3}. The central electron temperature is $T_e(0) = 3.1$ keV. Input parameters for this particular local L-mode simulation are listed in Table 2.

In the local GYRO simulation, the Miller equilibrium model is used [41] and $E \times B$ shear is included using the Waltz-Miller formula. The simulations are electrostatic, but GYRO can include electromagnetic effects. Gyrokinetic ions and drift-kinetic electrons are used, with realistic mass ratio ($\sqrt{m_i/m_e} = 60$). No dynamic impurity ions are included in this particular simulation, and quasineutrality forces ion and electron density

Table 2. Inputs for a local L-mode simulation that was used for synthetic diagnostic analysis. The simulation is run for parameters corresponding to an experimental position of $\rho = 0.5$. GYRO definitions and normalizations are used.

Parameter	Value
r/a	0.601
R/r	3.013
a (m)	0.218
n_e (10^{20}) m^{-3}	1.067
T_e (keV)	1.596
T_i (keV)	1.399
$a/L_{ne} = a(d\ln n_e/dr)$	0.600
$a/L_{Te} = a(d\ln T_e/dr)$	2.665
$a/L_{Ti} = a(d\ln T_i/dr)$	1.794
T_i/T_e	0.877
c_s/a (kHz)	1265
$\gamma_{E\times B}$ (c_s/a)	0.059
ν_{ei} (c_s/a)	0.078
ρ^*	0.00364
Z_{eff}	4.364
q	1.599
$\hat{s} = r(d\ln q/dr)$	1.241

fluctuations to be the same. In some of the global simulations used in the study (Section 6), dynamic impurity ions are included in trace amounts, but these do not impact the predicted main ion energy flux. The number of toroidal modes used in the local simulations is 16 with toroidal separation of $\Delta n = 8$, so that toroidal mode numbers range from 0 to 120. GYRO uses the binormal wavenumber, k_y, which is approximately the poloidal wavenumber, k_θ, and the range of toroidal mode numbers simulated corresponds to a binormal wavenumber range of $k_y\rho_s = [0, 1.16]$, where $k_y = nq/r$ and $q = rB_\phi/RB_\theta$ is the safety factor and r is the mid-plane minor radius of the flux surface and R is the midplane major radius of the flux surface. The integration time step used is $\Delta t = 0.007\ a/c_s$, and time-integration errors are less than 1×10^{-3} for electrons and less than 1×10^{-4} for ions. The numerical quality of the simulations is assessed by standard methods used in verification and modeling studies [42, 43].

4.1. Predicted Transport levels

The total energy flow, Q, for a species predicted by GYRO is defined in terms of the moment of the perturbed distribution function of the species, δf,

$$Q = \langle \int d^3v (mv^2/2) \delta f \delta v_x |\nabla r| \rangle dV(r)/dr, \tag{4}$$

where the angular brackets $\langle\rangle$ indicate a flux surface average. Here r is the midplane minor radius of the flux surface, $V(r)$ is the volume enclosed within the flux surface, and $\langle|\nabla r|\rangle dV(r)/dr$ is the surface area of the flux surface. The simulations must be run out to long times ($t > 700\ a/c_s$) to help ensure that the transport and the turbulence have reached statistical steady states that are insensitive to initial conditions [42].

The total normalized ion (blue-dashed) and electron (red-solid) energy fluxes for the L-mode simulation (inputs given in Table 2) are shown versus simulation time step, t, in Fig. 2 (a). The simulation data after $t > 350\ a/c_s$ are used to calculate turbulence quantities quoted in this paper.

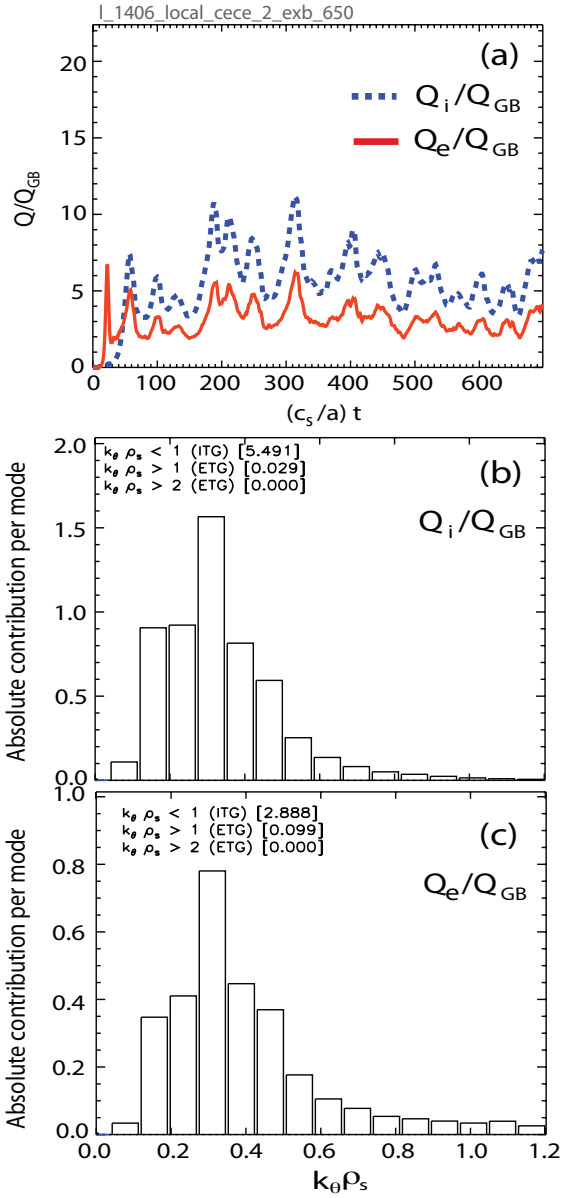

Figure 2. (Colour online) (a) The total ion (blue-dashed) and electron (red-solid) energy fluxes for the L-mode simulation (inputs given in Table 2) are shown versus simulation time step, t. The ion (b) and electron (c) energy fluxes in normalized units are plotted versus $k_\theta \rho_s < 1.2$.

Examining the spectral densities of the ion and electron energy fluxes, Q_i and Q_e, as a function of mode number, allows for a second check on the quality of the simulations - that the simulation parameters chosen are sufficient to capture transport driven by long-wavelength turbulence. An unrealistic simulation can run to completion but have

energy condensed at the largest wavenumber included in the simulation. A realistic simulation (for these cases where long wavelength ITG and trapped electron modes are unstable), in this study has very little contribution from high-k modes. The ion and electron heat fluxes in normalized units are plotted versus $k_\theta \rho_s$ in Fig. 2 (b) and (c), respectively. The ion and electron energy flows are well resolved with respect to wavenumber: the spectrum peaks at $k_\theta \rho_s = 0.3$ and there is little ($< 5\%$) contribution from high-k turbulence $k_\theta \rho_s > 1.0$.

For this local simulation, run at $\rho = 0.5$, the electron energy flux is in good agreement with experiment, $Q_e^{GYRO}/Q_e^{EXP} \approx 1.42$, but the ion energy flow is a factor of 10 above the experimental range, $Q_i^{GYRO}/Q_i^{EXP} \approx 12.5$. We note again that the experimental values for the ion temperature in this study are not based on measurements, but on TRANSP modeled ion temperature profiles. Scans of the local ion temperature gradient can be used to bring the simulation into better agreement in the ion channel [3, 12, 16]. We find that there is very little change in the electron energy flow and very little change in the electron temperature fluctuations when the ion temperature gradient is scanned, and this is discussed further in Section 6.

4.2. Turbulence Characteristics

For these L-mode parameters we find that the nonlinear turbulence is predominantly composed of ion modes, which can be seen by examining the frequency spectrum of the electron temperature fluctuations as a function of mode number, Fig. 3 (a) [43]. The midplane fluctuations are dominated by ITG modes ($\omega < 0$), with a peak at low frequency.

Linear stability analysis also indicates that the dominant instability is ITG for the plasmas considered here. Figure 3 (b) shows the linear growth rate (a/c_s) contours of the most unstable mode at $k_\theta \rho_s = 0.5$ at the radial location of $\rho = 0.5$. The solid white line indicates the boundary between modes rotating in the electron and ion diamagnetic drift direction. The unstable mode at $k_\theta \rho_s = 0.5$ is commonly found to be the peak in the low frequency linear growth rate spectrum and is chosen to be representative of characteristic, low-k plasma turbulence. For the simulation parameters considered in this study, the most unstable mode is found to rotate in the ion diamagnetic drift direction. For a fixed value of a/L_{T_e}, the linear growth rate of the dominant ion mode will increase (decrease) with an increase (decrease) in the value of the drive term, a/L_{T_i}, and the mode is identified as an ITG driven mode.

The linear stability analysis summarized in Fig. 3 (b) is performed for a wide range of normalized gradient scale lengths, only some of which correspond to experimental values. Values of a/L_{T_e} and a/L_{T_i} which are relevant for the plasmas considered in this paper are denoted by the white shaded oval region in Fig. 3 (b). The values of a/L_{Te} and a/L_{Ti} that correspond to the experimentally relevant nonlinear simulation result shown in 3 (a) are marked by the yellow cross.

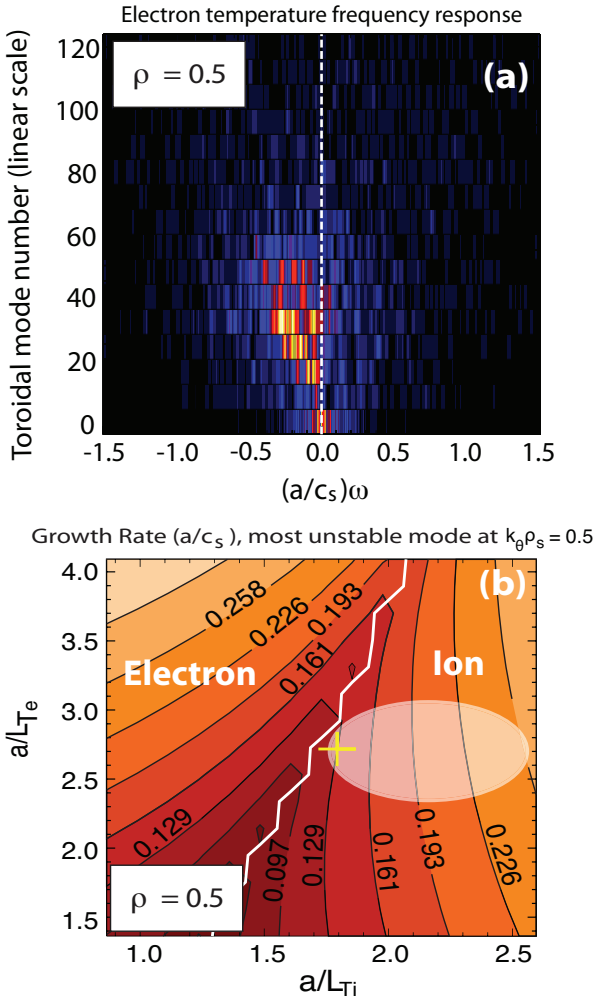

Figure 3. (Colour online) (a) The midplane electron temperature fluctuation frequency spectrum from local GYRO simulation at $\rho = 0.5$. (b) The growth rate (a/c_s) contours of the most unstable mode, evaluated at $k_\theta \rho_s = 0.5$, from the local simulation at $\rho = 0.5$. The values of a/L_{Te} and a/L_{Ti} that correspond to the simulation results in (a) is shown by the yellow cross. The white shaded region indicates the simulation ranges of gradient scale lengths.

4.2.1. Predicted fluctuation levels The predicted fluctuations are obtained from the density and energy moments of the distribution function. A kinetic pressure relation between density, temperature and pressure $p_e = T_e n_e$ is used to obtain the relation between internal energy fluctuations and pressure fluctuations, $\tilde{\epsilon} = 3/2\tilde{p}_e = 3/2(n_e\tilde{T}_e + \tilde{n}_e T_e)$ [44]. We define the normalized electron temperature fluctuations, $\delta T_e = \tilde{T}_e/T_e$ as

$$\tilde{T}_e/T_e = (2/3)\tilde{\epsilon}_e/p_e - \tilde{n}_e/n_e. \tag{5}$$

The GYRO predicted fluctuation level at $\rho = 0.5$ is $\tilde{T}_e/T_e = 1.52\%$, and is obtained from a box-average of the local simulation result. Global simulation results (not shown) are in agreement with this fluctuation level and also indicate that the fluctuation level increases with radius.

4.2.2. Predicted wavenumber spectrum The GYRO predicted poloidal wavenumber spectrum of electron temperature fluctuations in the core plasma at $\rho = 0.5$, from the local L-mode simulation (inputs in Table 2), is shown in Figure 4. This turbulence wavenumber spectrum peaks at $k_\theta \rho_s \approx 0.3$ or $k_\theta \approx 3.8$ cm^{-1}, which is in the same range where the peak in energy flux occurs, Figure 2. This indicates that electron temperature fluctuations are relevant for determining electron thermal transport in typical L-mode plasmas. This is also supported by the results of a large number of simulations, as discussed in Section 6, showing that the electron temperature fluctuation amplitude scales with the electron heat flux.

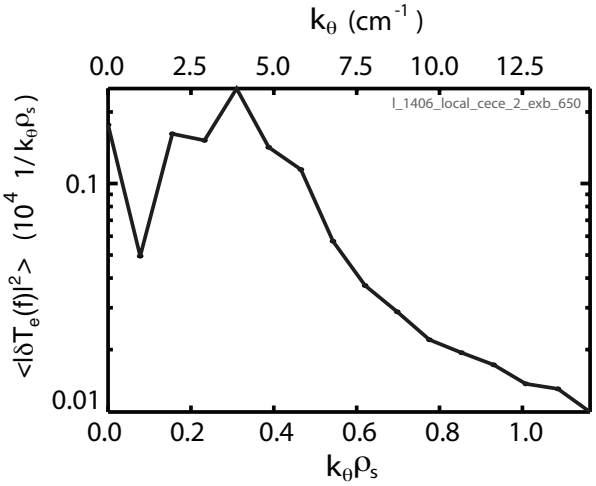

Figure 4. GYRO predicted poloidal wavenumber spectrum of electron temperature fluctuations in the core plasma $\rho = 0.5$, from the local L-mode simulation (Table 2).

4.2.3. Predicted radial correlation length From the simulation outputs, the time-averaged radial correlation coefficient function at the center of the simulation box is calculated. The radial correlation length, L_r, is defined as the $1/e$ folding width of the correlation coefficient function. The normalized radial correlation length is $L_r/\rho_s = 9$ in this simulation (L-mode, $\rho = 0.5$). For the value of $\rho_s = 7.5 \times 10^{-4}$ m, this gives a predicted correlation length of $L_r \approx 0.7$ cm.

4.2.4. Synthetic Diagnostic Model The predicted fluctuation level and correlation length discussed in the previous section are what would be measured if the diagnostic had perfect spatial resolution. In reality, the CECE diagnostic must average over the finite sample volume size. Taking these effects into account will produce more realistic predictions for the turbulence characteristics, and here we predict using synthetic diagnostics what would actually be measured in the experiment. The synthetic diagnostic model has been described in detail by Holland [12]. Here we briefly summarize the implementation steps.

First, in order to reconstruct synthetic $\tilde{T}_e/T_e$ fluctuations from the local GYRO results, fine radial and poloidal resolution are needed to model the effects of the finite sample volume size. The radial grid spacing of the simulation is $\delta x/\rho_s = 0.37$, with radial box size $110\rho_s$, such that radial resolution needed for the synthetic diagnostic reconstruction is always achieved. But to achieve the poloidal needed to reconstruct the synthetic diagnostic, the output from GYRO at 1024 theta points is saved (the default is 1). The vertical resolution of the simulation is defined as $\delta z = \kappa_r r \delta_\theta$, where kappa is the elongation of the flux surface [12]. If we use 1024 theta points, we have $\delta_\theta = 2\pi/1024 \approx 0.006$ radians, which corresponds to $\delta z/\rho_s \approx 0.13$, giving the needed resolution.

Second, the GYRO output at each reference point (r, θ) in the plasma reference frame must be transformed to the laboratory frame using a transform that depends on toroidal mode number, n,

$$f_{lab}(r, \theta, n, t) = f_{sim}(r, \theta, n, t) e^{in\omega_o t}, \tag{6}$$

where $\omega_o = -qcE_r/rB$ is the $\vec{E} \times \vec{B}$ rotation rate of the reference point [12]. The time resolution of the plasma frame spectrum is increased by a factor of four using linear interpolation before transformation to avoid aliasing.

Third, the spatial sensitivity of a single ECE signal is taken into account by modeling the sample volume in the radial and vertical directions as Gaussians using the Point Spread Function (PSF) of the form [12]

$$\psi_{CECE}(R - R_o, z - z_o) = e^{-[(R-R_o)/\Delta R]^2/2} e^{-[(z-z_o)/\Delta z]^2/2} \tag{7}$$

Here ΔR is the $1/e^2$ power diameter on the radial direction, determined by the natural linewidth of the EC emission and Δz is the $1/e^2$ power diameter on the vertical direction, determined by the antenna pattern. A second PSF with same Gaussian form is used to model the second ECE signal. The centers of the two PSFs can be positioned anywhere in the simulation domain, offset vertically, at an angle, or as shown in Figure 5 radially separated at the midplane.

Finally, to model the correlation analysis that is performed with the real CECE data, we produce synthetic arrays of pairs of closely spaced sample volumes and cross-correlate two spatially separated sample volumes to calculate the cross-power spectrum and rms fluctuation amplitude of the temperature fluctuations.

The contours of temperature fluctuations from GYRO are shown in Figure 5. The 10%, 50% and 90% contours of the PSFs are shown in white for two synthetic CECE signals separated by $\delta_R = 0.5$ cm. The sample volume sizes are in this case $\Delta R = 0.5$ in radial direction and $\Delta z = 1$ cm in the vertical direction.The radial spacing shown here would correspond to two IF filters with center frequencies separated by roughly 500 MHz. To ensure decorrelation of the thermal noise, $B_{if} < 250$ MHz.

4.2.5. Predicted cross-power spectrum of electron temperature fluctuations Using the PSF to spatially filter the raw GYRO output, we generate synthetic electron temperature fluctuation signals. The cross-power spectrum of the two radially separated

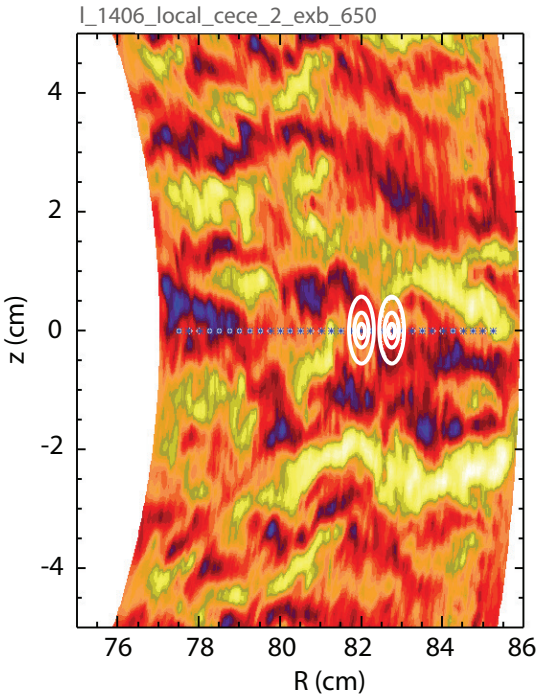

Figure 5. (Colour online) Nonlinear GYRO simulation results (local simulation, run at $\rho = 0.5$, inputs in Table 2) for a typical 1 MW RF-heated L-mode plasma in Alcator C-mod. Contours of predicted electron temperature fluctuations in the radial and vertical plane. Positions of the centers of synthetic diagnostic spatial transfer functions are shown as blue asterisks. The 90%, 50% and 10% power contours of the sample volumes (white) are shown for two CECE signals that are correlated to measure $\tilde{T}_e/T_e$. The CECE views the plasma from the outboard midplane, with an on axis view.

synthetic signals is calculated. This synthetic spectrum is the prediction for the Doppler-shifted laboratory frequency spectrum that would be measured using a CECE diagnostic.

In Figure 6 (a) the synthetic cross-power spectrum shown is from the local simulation (inputs in Table 2), which included $E \times B$ flows and shear. In this case, the predicted spectrum peaks at the frequency, $f = 100$ kHz, and is 150 kHz wide. The results of applying the PSF can be seen by comparing the unfiltered spectra to the spatially filtered spectra. When the signals are unfiltered, $\Delta z = 0$. When the vertical sample volume size is increased, the effects of the spatial filtering lead to a reduction in the amplitude of the cross-power spectrum. In Figure 6 (a) the vertical sample volume size, Δz, is increased from 0 cm (solid- black) to 1 cm (dashed-green), 2 cm (dashed-red), and 3 cm (dashed-blue). It has been described in detail previously how higher frequency information is filtered out more quickly than low frequency information; an effect that is due to the dominant vertical extent of the CECE sample volumes [12, 17]. Here we recover the same effect. The power spectrum is calculated with rather coarse frequency resolution 11 kHz in this case in order to maximize the number of realizations

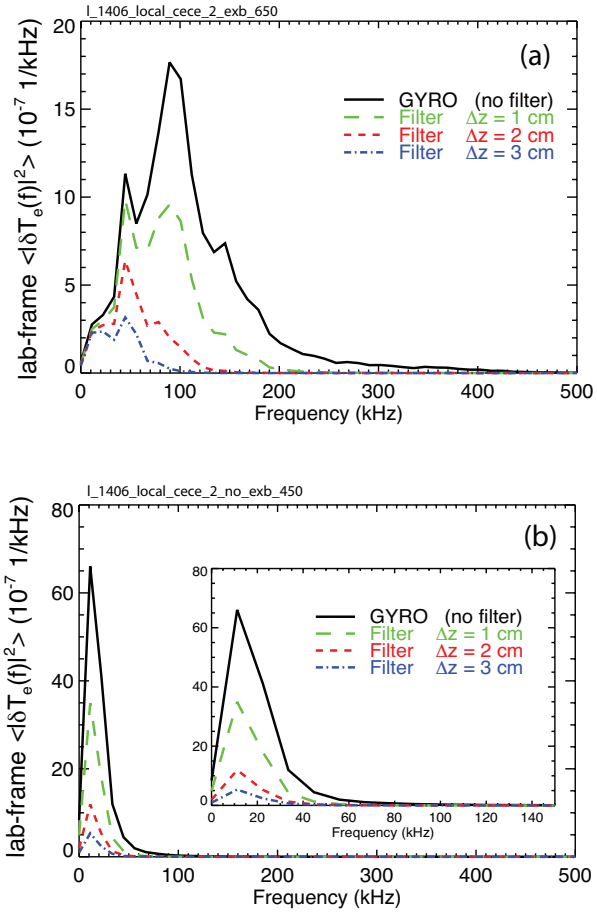

Figure 6. (Colour online) Synthetic diagnostic results from L-mode simulation at $\rho = 0.5$ (Inputs in Table 2). (a) Laboratory frame power spectrum from L-mode simulation with no $E \times B$ shear (b) Laboratory frame power spectrum from L-mode simulation with $E \times B$ shear included. The black solid curve is the result from GYRO with no sample volume model applied. When the vertical sample volume size, Δz is increased from 1 cm (large dashed-green) to 2 cm (small dashed-red) to 3 cm (dashed dot-blue), we find significant reductions in predictions for the measurable fluctuation level.

used in the ensemble average. We also performed the cross-power spectrum calculation with 5 kHz resolution and find no change in the overall shape of the spectrum or in the integrated fluctuation amplitude.

In Figure 6 (b) the synthetic cross-power spectrum shown is from the same local simulation (inputs in Table 2), but now with $E \times B$ shear turned off. With no background $E \times B$ flows, the power spectrum is much narrower because there is no Doppler shift in the laboratory frame, compared to the spectrum shown in Figure 6 (a). The cross-power spectrum is very narrow, peaking near $f = 20$ kHz with a width of 40 kHz. Again, as the spot-size is increased, the amplitude of the cross-power spectrum is reduced.

The fluctuation level, $\tilde{T}_e/T_e$ is calculated by integrating the synthetic cross-power spectrum between $f = 0 - 500$ kHz. The changes in measurable fluctuation level predicted by varying the vertical size of the PSF, Δz, are summarized in Table 3.

Table 3. Reduction in measurable fluctuation level predicted by increasing the vertical size of the point spread function. The vertical spot-size, Δz, is varied from 0 cm to 3 cm. The predicted fluctuation level is calculated by integrating the simulated cross-power spectrum between 0 and 500 kHz.

spot-size	$\tilde{T}_e/Te(\%)$ level with $E \times B$ shear	$\tilde{T}_e/Te(\%)$ level without $E \times B$ shear
$\Delta z = 0$ cm	1.29	1.26
$\Delta z = 1$ cm	0.93	0.87
$\Delta z = 2$ cm	0.57	0.50
$\Delta z = 3$ cm	0.40	0.34

When the the spot-size is $\Delta z = 3$ cm, GYRO predicts that the measured fluctuation level will be $\tilde{T}_e/T_e \approx 0.4\%$, which is at or near the practical sensitivity limit of a CECE diagnostic. When the spot-size is 1 cm, GYRO predicts that the measured fluctuation level will be $\tilde{T}_e/T_e \approx 0.93\%$, which is adequate to resolve the fluctuations above the sensitivity limit.

When the simulations include $E \times B$ shear, the main effect is a Doppler shift of the peak frequency and Doppler broadening of the frequency width of the laboratory frame power spectrum, e.g. comparing Figure 6 (a) and (b). Sensitivity scans for the cases considered here show that transport and fluctuation amplitude are not strongly affected by changes in E_r or $E \times B$ shear. As Table 3 shows, there is only a slight reduction in the fluctuation amplitude where $E \times B$ shear is included in the simulations.

4.2.6. Diagnostic Design Constraints from Synthetic Diagnostic Modeling The synthetic diagnostic results of the previous section can be used to (1) place an upper limit on the size of the antenna pattern needed at C-Mod and (2) motivate the need for a large video bandwidth in the CECE receiver.

The results shown in Figure 6 and Table 3 indicate that the past attempts at Alcator C-Mod did not detect any temperature fluctuations above the noise level because the sample volume of the diagnostic was too large. The $1/e^2$ power diameter for that past work was reported as $3 < \Delta z < 4$ cm [8, 9]. The GYRO modeling here shows that in order to detect fluctuation levels between $1.0 - 1.5\%$ at experimental $\rho = 0.5$, in a typical L-mode plasma, a spot-size with $\Delta z = 1$ cm is needed. The broad frequency spectrum due to Doppler shifts when $E \times B$ flow is included also suggests the CECE diagnostic should have a video bandwidth larger than $B_{vid} = 400 - 500$ kHz to resolve the turbulent fluctuations.

A check on these detailed modeling results can be done by making a simple empirical estimate for the required spot-size at C-Mod based on recent experimental results from DIII-D [17]. For typical L-mode plasmas at both C-Mod and DIII-D, $\rho* = 0.003 - 0.004$. At DIII-D, the CECE system has $\Delta z \approx 3$ cm and can observe fluctuations that peak near $k_\theta \rho_s^{peak} = 0.3$. Because the standard operating magnetic field at C-Mod ($B_T = 5.4$ T) is 2.7 times larger than at DIII-D ($B_T = 2.0$ T), it means that at C-mod the CECE sample volume size should be 2.7 times smaller than at DIII-D in order to detect fluctuations

with the same value of $k_\theta \rho_s^{peak} = 0.3$. Since the DIII-D CECE spot-size is roughly 3 cm, this means the C-Mod CECE spot-size needs to be roughly 1 cm, which is consistent with the GYRO modeling.

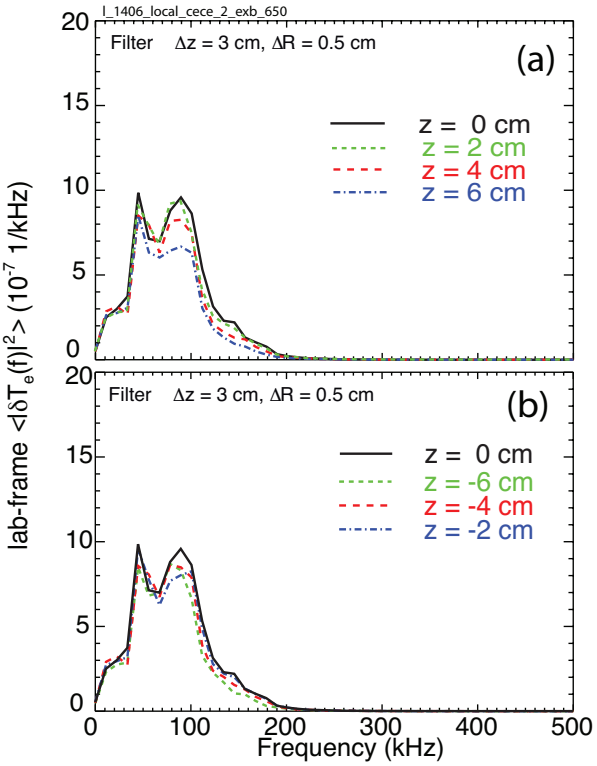

Figure 7. (Colour online) Synthetic diagnostic results from L-mode simulation at $\rho = 0.5$ (Inputs from Table 2). Lab frame spectra with $E \times B$ shear included for the fluctuations (a) above and (b) below the midplane. The sample volume size of $\Delta r = 0.5$ cm and $\Delta z = 1.0$ cm, with radial spacing of 0.5 cm was used here.

4.2.7. Effects of an off-midplane view The modeling so far has assumed that the diagnostic is viewing the plasma horizontally at the midplane along the major radius. This puts the sample volume that is probed by the diagnostic on the midplane. This viewing geometry may not be available given tight space limitations at Alcator C-Mod. For this reason, the new diagnostic may need to view the plasma at an angle with respect to the midplane. This would displace the sample volume above or below the midplane, which might affect the measured spectrum and fluctuation level level because past observations have shown poloidal asymmetries in the electron temperature fluctuation levels [45].

To model this effect, the synthetic signals are generated at several vertical positions in the simulation box. Using two CECE PSFs with $\Delta R = 0.5$ cm and $\Delta z = 1.0$ cm, separated radially by 0.5 cm, the synthetic cross-power spectra are calculated above and below the midplane. The results, shown in Figure 7, indicate that there is no significant variation in the measured fluctuation amplitude in the range ± 6 cm above or below

the midplane. This means that a CECE diagnostic with an off-midplane is expected to perform as well as one with an on-midplane view at C-Mod.

5. Sensitivity of Predicted Turbulence Characteristics

It is useful to understand how sensitive the predicted turbulence characteristics are to slight changes in the code input parameters. It has been shown that the outputs from simulations (e.g. heat fluxes, Q, and diffusivities, χ) are very sensitive to the input parameters when the input gradients are close to marginal stability [3]. Where the turbulence is predominantly ITG type, the ion heat flux specifically will be very sensitive to the input ion temperature gradient. To examine how sensitive the fluctuations are to changes in the ITG drive, a scan of input ion temperature gradient scale length, a/L_{Ti} was performed on the local simulation discussed in Section 4 (inputs in Table 2). The base value (Table 2) is $a/L_{Ti} = 1.794$ and is changed to $2, 3$ and 4 for the scan. It was not possible to obtain well-converged simulations for smaller values of input a/L_{Ti}.

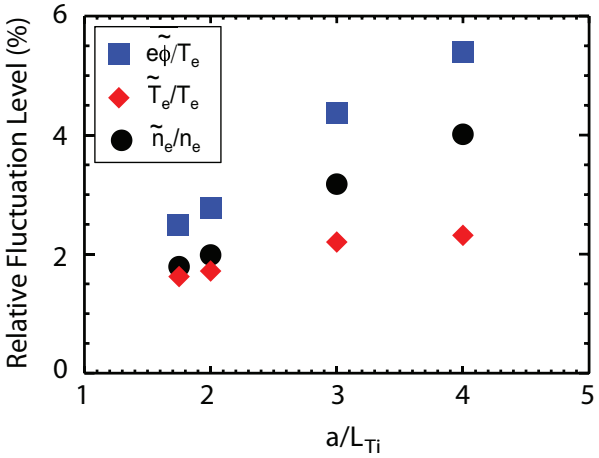

Figure 8. (Colour online) GYRO predicted fluctuation levels at $\rho = 0.5$ at the midplane as a function of input ion temperature gradient scale length, a/L_{Ti}.

Figure 8 shows the density fluctuation levels, electron temperature fluctuation levels, and electrostatic potential fluctuation levels at $\rho = 0.5$ at the midplane as a/L_{Ti} is increased. As the ITG drive term increases by a factor of 2, the electron temperature fluctuation amplitude increases by only 30%, from 1.5% up to 2%, but the density and potential fluctuations increase a factor of 2 with the increases in Q_i. For $a/L_{Ti} = 1.794$ and 2.0 the predicted ion energy fluxes remain in a reasonable range, $1.0 < Q_i^{GYRO}/Q_i^{EXP} < 10$. The input gradients for the higher drive simulations, $a/L_{Ti} = 3.0$ and 4.0, are unrealistic (outside experimental uncertainties). And in these two cases the predicted ion energy fluxes are not surprisingly large and unrealistic: $Q_i^{GYRO}/Q_i^{EXP} \approx 50$ and 100, respectively.

In the remainder of this section, we present results from both local and global GYRO simulations that were used to track how the predicted turbulence characteristics

Table 4. Ranges of simulation inputs for local and global L-mode simulations, at the center of the simulation box. GYRO definitions and normalizations are used.

Parameter	Range used in global simulations
n_e (10^{20}) m^{-3}	0.963 - 1.869
T_e (keV)	1.106 - 2.064
T_i (keV)	1.117 - 1.663
$a/L_{ne} = a(d\ln n_e/dr)$	0.600 - 1.506
$a/L_{Te} = a(d\ln T_e/dr)$	1.216 - 3.258
$a/L_{Ti} = a(d\ln T_i/dr)$	1.445 - 4.000
T_i/T_e	0.740 - 1.046
c_s/a (kHz)	1034 - 1442
ν_{ei} (c_s/a)	0.053 - 0.078
ρ^*	0.0034 - 0.0044
Z_{eff}	1.878 - 4.364
q	1.491 - 1.840
$\hat{s} = r(d\ln q/dr)$	0.780 - 1.415

varied across many simulations. We find here that overestimates in ion energy flow do not change interpretation of the results of Section 4 , since in these plasmas the electron temperature fluctuations do not scale strongly with ion energy flow.

5.1. Global Simulations Parameters

The database of GYRO simulations used for the diagnostic design first included only local simulations, but was expanded significantly by including global simulations. The input files for the runs were prepared using experimental profiles as input as discussed in Section 3, i.e. using the output of TRANSP and the data translator (trgk) developed at PPPL.

The global, nonlinear GYRO simulations considered in this paper were performed using the real ion/electron mass ratio and kinetic electrons. The simulations were performed with $N_n = 8$ toroidal modes, separation $\Delta n = 10$, box size $130\rho_s$, covering roughly the experimental radial range $0.35 < \rho < 0.75$, with the center at $\rho \approx 0.5$; or with $N_n = 16$ toroidal modes, separation of $\Delta n = 7$, box size $80\rho_s$, covering roughly the experimental radial range $0.3 < \rho < 0.5$, with center at $\rho \approx 0.4$. Due to lack of available rotation data, parallel velocity and $E\times B$ effects were not included. Low levels of rotation are typically observed in similar L-mode plasmas but based on results from the local simulations discussed in Section 4 and summarized in Table 3, the effects of including equilibrium rotation and $E \times B$ shear in the global simulations are expected to be negligible. Given the the ITG dominated nature of these plasmas, high-k contributions were ignored and these simulations included maximum values of $k_\theta\rho_s$ between .85 and 1.2. Ranges of input parameters for all the global simulations are given in Table 4. The values listed in Table 4 are taken at the center of the simulation box, which varies, but corresponds to the core experimental radial region of interest, $0.4 < \rho < 0.5$. The predicted values of heat transport and electron temperature fluctuation characteristics

are taken from the global simulation at the center of the box.

Figure 9 summarizes the results from over thirty local and global L-mode simulations with ranges of input parameters given in Table 4. These results show that predicted electron energy flux remains realistic, within a factor of two of the experimental values, $0.5 < Q_e^{GYRO}/Q_e^{EXP} < 2.0$ for all cases. In contrast, the ion energy flux varies by two orders of magnitude.

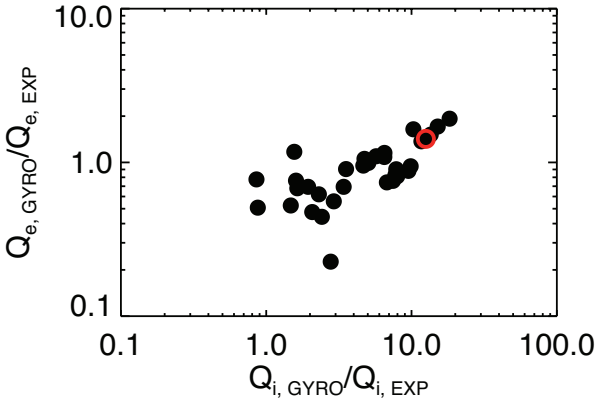

Figure 9. (Colour online) Ratio of predicted electron energy flux to experimental value is compared to the ratio of predicted ion energy flux to experimental value for more than thirty local and global L-mode simulations. The local simulation discussed in Section 4 is shown with the red circle.

5.2. Scaling of turbulence characteristics with predicted heat fluxes

The predicted values for the fluctuation level, $\tilde{T}_e/T_e$, peak poloidal wavenumber, $k_\theta \rho_s$, and the radial correlation length, L_r are collected from many global GYRO simulations of L-mode plasmas in order to determine how sensitive the parameters are to slight changes in simulation parameters.

Shown in Fig. 10 (a) the predicted electron temperature fluctuations fall in the range $\tilde{T}_e/T_e = 0.9 - 2.0\%$ when the predicted electron energy flux is in a realistic range, $0.5 < Q_e^{GYRO}/Q_e^{EXP} < 2.0$. There is also a very clear scaling of the fluctuation level with electron energy flux, which is not surprising given that electron temperature fluctuations can contribute significantly to electron thermal transport [17]. It can be seen in Fig. 10 (b) that the ion energy flux ratio, Q_i^{GYRO}/Q_i^{EXP} varies by of an order of magnitude when the electron temperature fluctuations vary only a factor of two. There is no strong scaling of electron temperature fluctuation level with ion energy flux.

Shown in Fig. 11 (a), the predicted peak value of $k_\theta \rho_s$ falls in the range $0.2 < k_\theta \rho_s < 0.5$ when the predicted electron energy flux is in a realistic range, $0.5 < Q_e^{GYRO}/Q_e^{EXP} < 2.0$, and there is no clear scaling as in the case of fluctuation amplitude. The peak value is taken from the wavenumber spectrum from each simulation (e.g. Fig. 4).

Shown in Fig. 12 (a), the predicted radial correlation length of electron temperature

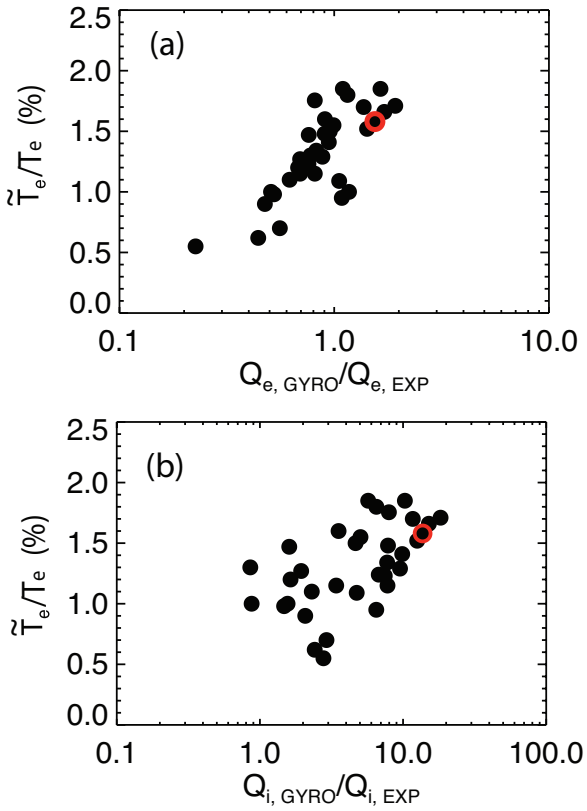

Figure 10. (Colour online) Fluctuation level plotted against (a) Q_e^{GYRO}/Q_e^{EXP} and (b) Q_i^{GYRO}/Q_i^{EXP} from series of L-mode simulations. The open red circle corresponds to the local simulation from Section 4 (b)

fluctuations falls in the range $3 < L_r/\rho_s < 10$ when $0.5 < Q_e^{GYRO}/Q_e^{EXP} < 2.0$. Like the peak wavenumber, there is no clear scaling with electron energy flux. Similarly, as Figure 12 (b) shows, large order of magnitude changes in the ion energy flux ratio, Q_i^{GYRO}/Q_i^{EXP}, results in no clear scaling of the radial correlation length.

The results from the global simulations show that as heat flux increases, so does the fluctuation amplitude. Electron temperature fluctuation level does scale strongly with electron heat flux, but scales weakly with ion heat flux. The radial correlation length and the peak wavenumber of the fluctuations do not exhibit any scaling with heat flux in either channel, even when the heat flux changes by an order of magnitude.

6. Discussion and Conclusions

In the present work, nonlinear gyrokinetic simulations and synthetic diagnostics are used to quantitatively predict electron temperature fluctuations in the core plasma at Alcator C-Mod in order to guide the design of a new correlation electron cyclotron emission (CECE) diagnostic. Results from nonlinear GYRO simulations of typical L-mode Alcator C-Mod plasmas heated with 1-2 MW of RF power show that the core turbulence is propagating in the ion diamagnetic drift direction. Linear stability analysis

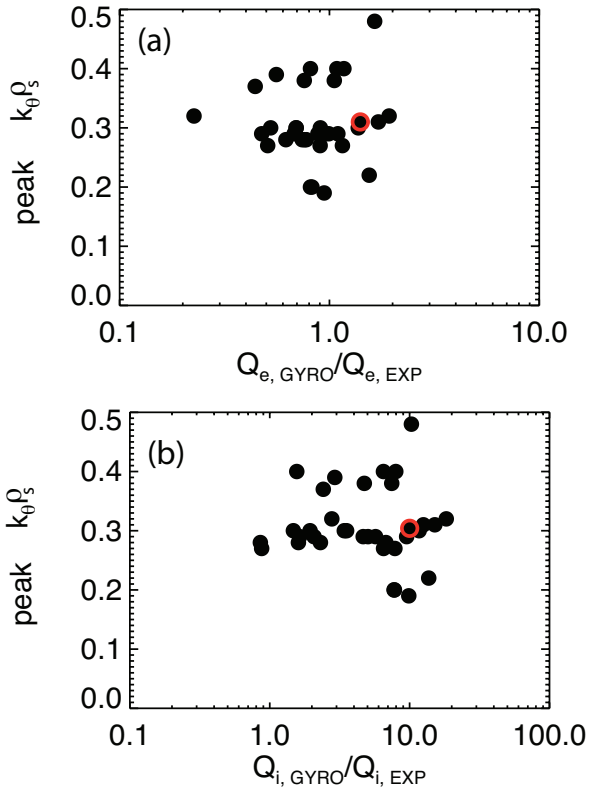

Figure 11. (Colour online)Peak values of $k_\theta\rho_s$ plotted against (a) Q_e^{GYRO}/Q_e^{EXP} and (b) Q_i^{GYRO}/Q_i^{EXP} from series of L-mode simulations. The open red circle corresponds to the local simulation from Section 4.

identifies unstable ITG modes and trapped electron modes in the plasma, where the ITG mode is the dominant linear instability. When using the simulations to predict turbulence characteristics, we only used realistic simulations: those that could match experimental electron heat transport to within a factor of two.

In these cases, the electron temperature fluctuation amplitude is predicted to be in the range $0.5\% < \tilde{T}_e/T_e < 2.0\%$ at mid-radius, $\rho = 0.5$. The predicted fluctuation wavenumber spectrum peaks in the range $0.2 < k_\theta\rho_s < 0.4$ and the radial correlation length of electron temperature fluctuations is between $0.4 < L_r < 0.8$ cm, scaling as $(2-10)\rho_s$. Results from the simulations show that electron temperature fluctuations are transport relevant, and are strongly correlated with electron energy transport. The modeling results presented in this paper show that a CECE diagnostic capable of measuring transport-relevant, long-wavelength ($k_\theta\rho_s < 0.5$) electron temperature fluctuations is feasible at Alcator C-Mod.

Here we summarize the design guidelines prescribed by the GYRO modeling.

First, the predicted radial correlation length is small, less than 1 cm. This means that narrow IF filters with bandwidth in the range $100 < B_{if} < 250$ MHz (i.e. much narrower than the natural linewidth $1-2.5$ GHz) should be used in the new diagnostic in order to ensure that the filters can be disjoint in frequency space, but still be within a correlation length of the turbulence.

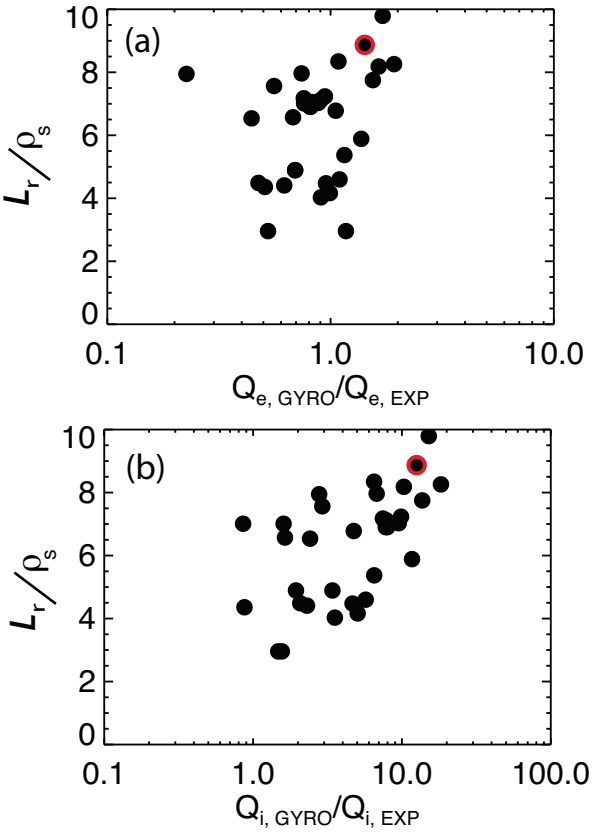

Figure 12. (Colour online) Radial correlation length, L_r, normalized to ρ_s plotted against (a) Q_e^{GYRO}/Q_e^{EXP} and (b) Q_i^{GYRO}/Q_i^{EXP} from series of L-mode simulations. The open red circle corresponds to the local simulation from Section 4.

Second, synthetic diagnostics are used to model the frequency spectrum of the turbulence in the laboratory frame. In order to resolve the turbulence, the video bandwidth of the diagnostic but be wider than the predicted frequency spectrum of the turbulence. A choice of $B_{vid} > 500$ kHz is suggested by the modeling results. Given the possibility of larger $E \times B$ flows in C-Mod plasmas (e.g. during H-mode plasmas or during L-mode plasmas with mode conversion flow drive experiments, it is best to select a wider video bandwidth, $B_{vid} = 1$ MHz.

Third, synthetic diagnostics are used to model effects of the finite sample volume size of the proposed CECE diagnostic. The results show that if the sample volume has a radial 90% power diameter of 0.5 cm and a vertical 90% power diameter of 1 cm, the CECE diagnostic would be sensitive to 1% electron temperature fluctuations at $\rho = 0.5$. However, once the vertical diameter is increased to 3 cm, the measurable fluctuation level drops to $0.3 - 0.4\%$, which will be just at the sensitivity limit of the diagnostic if the choices of $B_{vid} = 1$MHz and $100 < B_{if} < 250$ MHz are used. This result indicates that the new CECE system must use Gaussian optics that provide a 1 cm spot-size in the plasma. This modeling result also suggests that the large vertical sample volume size ($3-4$ cm) is the most likely explanation for why past CECE measurement attempts

did not resolve turbulence at Alcator C-Mod [10].

Fourth, the GYRO results also show that within a 6 cm range above and below the midplane there is no significant variation in the fluctuation level. This is important because the proposed diagnostic may be forced to measure the turbulence at locations several centimeters above or below the midplane given constraints on available port-space.

For this study, we restricted ourselves to simulations of typical L-mode plasma parameters, where a large number of realistic simulations (> 30) could be obtained. It would also have been possible to use simulations of H-mode or Ohmic plasmas in an extensive design study, but we did not do this because there were fewer extant GYRO simulations that showed good agreement with experiment for these parameters [16, 18].

Once the CECE diagnostic is installed at C-Mod, it can be used to study turbulence and turbulent transport in the core plasma. Electron temperature fluctuation measurements provide information about electron energy transport directly, and when combined with models, can provide indirect information about ion energy transport, particle and momentum transport. The results from the present modeling work can be tested in future experiments.

If temperature fluctuations above the sensitivity limit of the diagnostic are observed in plasmas similar to those considered in this feasibility study, this will already provide a test of the simulation predictions presented here. A more detailed test of the predictions from this study could include examining the trend that electron temperature fluctuations in typical L-mode plasmas are insensitive to the ion heat flux, but are very sensitive to the electron heat flux. This prediction could be tested in future experiments by varying the amount of ion and electron heating. The predicted radial correlation length from the GYRO modeling is similar to the linewidth of the ECE in Alcator C-Mod, which is an interesting result that is consistent with past experimental observations on other tokamaks [23] and could be explored in future experiments on C-Mod. The data from the CECE diagnostic could also be used to study low-density Ohmic plasmas in Alcator C-Mod [18], where GYRO disagrees with experiment. The new CECE diagnostic could be used to study core turbulence in plasmas with internal transport barriers where TEM is the dominant instability [46].

One area for future modeling work is the development of an improved synthetic CECE diagnostic, i.e. one which takes into account effects due to refraction and emission/absorption of EC emission. We note that contamination of an ECE radiometer signal with density fluctuations due to refractive effects can potentially pose problems with an off-axis view. We have not considered these effects in the current work, but they are to be included in future modeling efforts. With the synthetic diagnostic used in this work, the radial width of the spot-size is modeled as a Gaussian. In reality, due to relativistic broadening the linewidth is not actually a Gaussian in shape, but has a tail extending in the region of smaller major radii (higher temperature) [19]. An improved synthetic diagnostic model that takes the emission and reabsorption of EC radiation into account (solving the radiation transport equation) is needed to fully model the shape

of the linewidth. This updated model will be used in the future to explore planned measurements of the radial correlation length, which may be limited by the natural linewidth of the EC emission, rather than the turbulence [23].

Acknowledgments

AEW gratefully acknowledges insightful discussions with D. Ernst about turbulence as observed in nonlinear gyrokinetic simulations of Alcator C-Mod plasmas, as well as helpful comments and suggestions from A. Hubbard, I. H. Hutchinson and P. Phillips on the topic of ECE measurement interpretation. This work is supported by the US Department of Energy under DE-FC02-99ER54512-CMOD. Computer simulations using GYRO were carried out on the MIT PSFC parallel AMD Opteron/Infiniband cluster Loki.

[1] E. J. Doyle and et al. Chapter 2: Plasma confinement. *Nucl. Fusion*, 47:S18–S127, 2007.

[2] A. J. Brizard and T. S. Hahm. Foundations of nonlinear gyrokinetic theory. *Rev. Mod. Phys.*, 79:421, 2007.

[3] J. Candy and R. E. Waltz. Anomalous transport scaling in the diii-d tokamak matched by supercomputer simulation. *Phys. Rev. Lett.*, 91(4):045001, Jul 2003.

[4] X. Garbet, Y. Idomura, L. Villard, and T. H. Watanabe. Gyrokinetic simulations of turbulent transport. *Nuclear Fusion*, 50:043002, 2010.

[5] A. E. White and et al. Measurements of the cross-phase angle between density and electron temperature fluctuations and comparison with gyrokinetic simulations. *Phys. Plasmas*, 17:056103, 2010.

[6] T. A. Casper, J. Jayakumar, M. A. Makowski, and R. Ellis. Design aspects of a mse diagnostic for iter. *Rev. Sci. Instrum.*, 75:4193, 2004.

[7] A. Malaquias, M. von Hellermann, S. Tugarinov, P. Lotte, N. Hawkes, M. Kuldkepp, E. Rachlew, A. Gorshkov, A. Costley C. Walker, and G. Vayakis. Active beam spectroscopy diagnostics for iter: present status (invited). 2004.

[8] J. W. Heard, C. Watts, R. F. Gandy, P. E. Phillips, G. Cima, R. Chatterjee, A. Blair, A. Hubbard, C. W. Domier, and Jr. N. C. Luhmann. High resolution electron cyclotron emission temperature profile and fluctuation diagnostic for alcator c-mod. *Review of Scientific Instruments*, 70(1):1011–1013, 1999.

[9] R. Chatterjee, P.E. Phillips, J. Heard, C. Watts, R. Gandy, and A. Hubbard. High resolution ece radiometer for electron temperature profile and fluctuation measurements on alcator c-?mod. *Fusion Engineering and Design*, 53.

[10] C. Watts, H. J. Hartfuss, and M. Haese. Comparison of different methods of electron cyclotron emission-correlation radiometry for the measurement of temperature fluctuations in the plasma core. *Review of Scientific Instruments*, 75:3177–3184, 2004.

[11] R. V. Bravenec and W. M. Nevins. System for simulating fluctuation diagnostics for application to turbulence computations. *Review of Scientific Instruments*, 77:015101, 2006.

[12] C. Holland, J. Candy, R. Waltz, A.E. White, G.R. McKee, M.W. Shafer, L. Schmitz, and G. R. Tynan. Validating simulations of core tokamak turbulence: Current status and future directions. *Phys. Plasmas*, 16:052301, 2008.

[13] E. Marmar, A. Bader, M. Bakhtiari, H. Barnard, W. Beck, I. Bespamyatnov, A. Binus, P. Bonoli, B. Bose, M. Bitter, I. Cziegler, G. Dekow, A. Dominguez, B. Duval, E. Edlund, D. Ernst, M. Ferrara, C. Fiore, T. Fredian, A. Graf, R. Granetz, M. Greenwald, O. Grulke, D. Gwinn, S. Harrison, R. Harvey, T.C. Hender, J. Hosea, K. Hill, N. Howard, D.F. Howell, A. Hubbard, J.W. Hughes, I. Hutchinson, A. Ince-Cushman, J. Irby, V. Izzo, A. Kanojia, C. Kessel, J.S. Ko,

P. Koert, B. LaBombard, C. Lau, L. Lin, Y. Lin, B. Lipschultz, J. Liptac, Y. Ma, K. Marr, M. May, R. McDermott, O. Meneghini, D. Mikkelsen, R. Ochoukov, R. Parker, C.K. Phillips, P. Phillips, Y. Podpaly, M. Porkolab, M. Reinke, J. Rice, W. Rowan, S. Scott, A. Schmidt, J. Sears, S. Shiraiwa, A. Sips, N. Smick, J. Snipes, J. Stillerman, Y. Takase, D. Terry, J. Terry, N. Tsujii, E. Valeo, R. Vieira, G. Wallace, D. Whyte, J.R. Wilson, S. Wolfe, G. Wright, J. Wright, S. Wukitch, G. Wurden, P. Xu, K. Zhurovich, J. Zaks, and S. Zweben. Overview of the alcator c-mod research program. *Nuclear Fusion*, 49(10):104014, 2009.

[14] J. Candy and R. E. Waltz. *J. Comput. Phys.*, 186:545, 2003.

[15] A. Casati, T. Gerbaud, P. Hennequin, C. Bourdelle, J. Candy, F. Clairet, X. Garbet, V. Grandgirard, Ö. D. Gürcan, S. Heuraux, G. T. Hoang, C. Honoré, F. Imbeaux, R. Sabot, Y. Sarazin, L. Vermare, and R. E. Waltz. Turbulence in the tore supra tokamak: Measurements and validation of nonlinear simulations. *Physical Review Letters*, 102(16):165005, 2009.

[16] L. Lin, M. Porkolab, E. M. Edlund, J. C. Rost, C. L. Fiore, M. Greenwald, Y. Lin, D. R. Mikkelsen, N. Tsujii, and S. J. Wukitch. Studies of turbulence and transport in alcator c-mod h-mode plasmas with phase contrast imaging and comparisons with gyro. *Physics of Plasmas*, 16(1):012502, 2009.

[17] A. E. White, L. Schmitz, G. R. McKee, C. Holland, W. A. Peebles, T. A. Carter, M. W. Shafer, M. E. Austin, K. H. Burrell, J. Candy, J. C. DeBoo, E. J. Doyle, M. A. Makowski, R. Prater, T. L. Rhodes, G. M. Staebler, G. R. Tynan, R. E. Waltz, and G. Wang. Measurements of core electron temperature and density fluctuations in diii-d and comparison to nonlinear gyrokinetic simulations. *Phys. Plasmas*, 15:056116, 2008.

[18] L Lin, M Porkolab, E M Edlund, J C Rost, M Greenwald, N Tsujii, J Candy, R E Waltz, and D R Mikkelsen. Studies of turbulence and transport in alcator c-mod ohmic plasmas with phase contrast imaging and comparisons with gyrokinetic simulations. *Plasma Physics and Controlled Fusion*, 51(6):065006, 2009.

[19] I. H. Hutchinson. *Principles of Plasma Diagnostics*. Cambridge University Press, 1987.

[20] S. E. Kissel T. C. hsu and I. H. Hutchinson. A novel fast scan michelson interferometer for ece diagnostic applications on alcator c-mod. *Proceedings of the 7th Joint Workshop and IAEA Technical Committee on Electron Cyclotron Emission and Electron Cyclotron Resonance Heating*, page 31, 1990.

[21] P. J. O'Shea, A. E. Hubbard, and the Alcator C-Mod Group. Nine channel polychromator for fast t_e measurements on alcator c-mode. *Proc. 9th Joint Workshop on ECE and ECRH (Borrego Springs, USA, 1995) ed. J. LOHR (World Scientific, Singapore, 1995)*, page 7, 1995.

[22] H. J. Hartfuss, T. Geist, and M. Hirsch. Heterodyne methods in millimetre wave plasma diagnostics with applications to ece, interferometry and reflectometry. *Plasma Phys. Control. Fusion*, 39:1693–1769, 1997.

[23] C. Watts. *Fusion Sci. & Technol*, 52:176, 2007.

[24] G. Bekefi. *Radiation Processes in Plasmas*. John Wiley and Sons, NY, 1966.

[25] G. Cima, R. V. Bravenec, A. J. Wootton, T. D. Rempel, R. F. Gandy, C. Watts, and M. Kwon. Core temperature fluctuations and related heat transport in the texas experimental tokamak-upgrade. *Physics of Plasmas*, 2(3):720–726, 1995.

[26] S. Sattler and H. J. Hartfuss. Intensity interferometry for measurement of electron temperature fluctuations in fusion plasmas. *Plasma Phys. Control. Fusion*, 35:1285–1306, 1993.

[27] V. S. Udintsev, M. Goniche, J. L. Segui, G. Giruzzi, D. Molina, F. Turco, G. T. A. Huysman, P. Maget, and Tore Supra Team. *Fusion Science and Technology*, 50:508, 2006.

[28] R. V. Bravenec and A. J. Wootton. Effects of limited spatial resolution on fluctuation measurements (invited). *Review of Scientific Instruments*, 82:802, 1995.

[29] Paul F. Goldsmith. *Quasioptical Systems: Gaussian Beam Quasioptical Propogation and Applications, publisher = Institute of Electrical and Electronics Engineers, Inc. NY, year = 1998, pages=36.*

[30] G R Tynan, A Fujisawa, and G McKee. A review of experimental drift turbulence studies. *Plasma*

Physics and Controlled Fusion, 51(11):113001 (77pp), 2009.

[31] S. Sattler, H. J. Hartfuss, and W7-AS Team. Experimental evidence for electron temperature fluctuations in the core plasma of the w7-as stellarator. *Physical Review Letters*, 72:653, 1994.

[32] R. E. Waltz, J. Candy, and M. Fahey. Coupled ion temperature gradient and trapped electron mode to electron temperature gradient mode gyrokinetic simulations. *Physics of Plasmas*, 14(5):056116, 2007.

[33] T. Görler and F. Jenko. Scale separation between electron and ion thermal transport. *Phys. Rev. Lett.*, 100(18):185002, May 2008.

[34] *http://meetings.aps.org/link/BAPS.2010.DPP.PO4.9*, 2010.

[35] J. W. Hughes, D. Mossessian, K. Zhurovich, M. DeMaria, K. Jensen, and A. Hubbard. Thomson scattering upgrades on alcator c-mod. *Review of Scientific Instruments*, 74(3):1667–1670, 2003.

[36] A. Ince-Cushman, J. E. Rice, S. G. Lee, M. Bitter, M. Reinke, and Y. Podpaly. Preliminary results from the soft x-ray crystal spectrometer on alcator c-mod. *Review of Scientific Instruments*, 77(10):10F321, 2006.

[37] L.L. Lao, J.R. Ferron, R.J. Groebner, W. Howl, H. St. John, E.J. Strait, and T.S. Taylor. Equilibrium analysis of current profiles in tokamaks. *Nuclear Fusion*, 30(6):1035, 1990.

[38] Transp documentation website.

[39] R.J Goldston, D.C McCune, H.H Towner, S.L Davis, R.J Hawryluk, and G.L Schmidt. New techniques for calculating heat and particle source rates due to neutral beam injection in axisymmetric tokamaks. *Journal of Computational Physics*, 43(1):61 – 78, 1981.

[40] C.C. Petty, T.C. Luce, J.C. DeBoo, R.E. Waltz, D.R. Baker, and M.R. Wade. Scaling of heat transport with beta in the diii-d tokamak. *Nuclear Fusion*, 38:1183, 1998.

[41] R. L. Miller, M. S. Chu, J. M. Greene, Y. R. Lin-Liu, and R. E. Waltz. Noncircular, finite aspect ratio, local equilibrium model. *Phys. Plasmas*, 5:973, 1998.

[42] W. M. Nevins, S. E. Parker, Y. Chen, J. Candy, A. Dimits, W. Dorland, G. W. Hammett, and F. Jenko. Verification of gyrokinetic delta f simulations of electron temperature gradient turbulence. *Physics of Plasmas*, 14(8):084501, 2007.

[43] J. E. Kinsey, R. E. Waltz, and J. Candy. The effect of safety factor and magnetic shear on turbulent transport in nonlinear gyrokinetic simulations. *Physics of Plasmas*, 13(2):022305, 2006.

[44] R. E. Waltz, M. E. Austin, K. H. Burrell, and J. Candy. Gyrokinetic simulations of off-axis minimum-q profile corrugations. *Physics of Plasmas*, 13(5):052301, 2006.

[45] Christopher Watts, R. F. Gandy, G. Cima, R. V. Bravenec, D. W. Ross, A. J. Wootton, A. Ouroua, J. W. Heard, T. P. Crowley, P. M. Schoch, D. L. Brower, Y. Jiang, B. Deng, C. W. Domier, and Jr. N. C. Luhmann. Poloidal asymmetry and gradient drive in core electron density and temperature fluctuations on the texas experimental tokamak-upgrade. *Physics of Plasmas*, 3(5):2013–2021, 1996.

[46] D. R. Ernst, N. Basse, W. Dorland, C. L. Fiore, L. Lin, A. Long, M. Porkolab, K. Zeller, , and K. Zhurovich. Identification of tem turbulence through direct comparison of nonlinear gyrokinetic simulations with phase contrast imaging density fluctuation measurements. *IAEA Fusion Energy Conference, Chengdu, China, 1621 October 2006*, IAEA-CN-149/TH/1-3, 2006.